Sensitivity to Gauge-Mediated Supersymmetry Breaking Models of the Fermilab Upgraded Tevatron Collider

Jianming Qian

Department of Physics, The University of Michigan
Ann Arbor, Michigan 48109
Email: qianj@umich.edu

This paper discusses supersymmetry discovery potential of the upgraded DØ experiment at the Tevatron $p\bar{p}$ collider. Six final states with large transverse energy (momentum) leptons or photons (with or without large transverse momentum imbalances) are studied. These final states are expected to have small backgrounds and are thereby ideal for new physics searches. Implications of the analyses of these final states on Gauge Mediated Supersymmetry Breaking models are discussed for integrated luminosities of 2 and 30 fb^{-1}. This study demonstrates that a large class of supersymmetry models can be probed at the upgraded Tevatron.

I. INTRODUCTION

This paper summarizes the work done for the Tevatron Run II Higgs/Supersymmetry workshop [1] on the supersymmetry models with Gauge Mediation/Low Scale Supersymmetry Breaking (GMSB) [2]. Six final states in which new physics might manifest itself are investigated using the parameters of the upgraded DØ detector [3]. All of these final states are expected to have small physics and instrumentation backgrounds. Implications of the analyses of these final states in future Tevatron runs on the minimal (and not-so-minimal) GMSB models are discussed. Estimated discovery reaches in the supersymmetry parameter space are presented.

II. OBJECT IDENTIFICATION

Due to a large number of Monte Carlo (MC) events generated, no detector simulation is done for supersymmetry signals. All studies described in this paper except those extrapolated from Run I analyses are carried out at the particle level of the ISAJET MC program [4]. A 2 TeV Tevatron center-of-mass energy is assumed throughout the studies. Leptons ($\ell = e, \mu$) and photons (γ) are 'reconstructed' from the generated particle list by requiring them to have transverse energy (E_T) or momentum (p_T) greater than 5 GeV and to be within the pseudorapidity ranges:

e: $|\eta| < 1.1$ or $1.5 < |\eta| < 2.0$;

μ: $|\eta| < 1.7$;

γ: $|\eta| < 1.1$ or $1.5 < |\eta| < 2.0$.

These fiducial ranges are dictated by the coverages of the electromagnetic calorimeter and the central tracker of the DØ detector. Furthermore, the leptons and photons must be isolated. Additional energy in a cone with a radius $\mathcal{R} \equiv \sqrt{(\Delta\phi)^2 + (\Delta\eta)^2} = 0.5$ in $\eta - \phi$ space around the lepton/photon is required to be less than 20% of its energy.

Jets are reconstructed using a cone algorithm with a radius $\mathcal{R} = 0.5$ in $\eta - \phi$ space and are required to have $E_T^j > 20$ GeV and $|\eta^j| < 2.0$. All particles except neutrinos, the lightest supersymmetric particles (LSP), and the identified leptons and photons are used in the jet reconstruction. The transverse momentum imbalance ($\not\!\!E_T$) is defined to be the total transverse energy of neutrinos and the LSPs.

Energies or momenta of leptons, photons and jets of Monte Carlo events are taken from their particle level values without any detector effect. Smearing of energies or momenta of leptons, photons and jets according to their expected resolution typically changes signal efficiencies by less than 10% relatively and therefore has negligible effect on the study.

The reconstruction efficiencies are assumed to be 90% for leptons and photons. For the purpose of background estimations, the probability ($\mathcal{P}$) for a jet to be misidentified as a lepton ($j \to \ell$) or a photon ($j \to \gamma$) is assumed to be 10^{-4}. The probability for an electron to be misidentified as a photon ($e \to \gamma$) is assumed to be 4×10^{-4}, These probabilities are

a factor of three or more smaller than those obtained in Run I [*]. With a new magnetic central tracking system and a fine-segmented preshower detector, they should be achievable in Run II.

In Run I, tagging of b-jets was limited to the use of soft muons in DØ. Secondary vertex tagging of b-jets will be a powerful addition in Run II. For the studies described below, a tagging efficiency of 60% is assumed for those b-jets with $E_T > 20$ GeV and $|\eta| < 2.0$. The probability $\mathcal{P}(j \to b)$ for a light-quark or gluon jet to be tagged as a b-jet is assumed to be 10^{-3}. These numbers are optimistic extrapolations of what CDF achieved in Run I.

Heavy stable charged particles can be identified [5,6] using their expected large ionization energy losses (dE/dx) in the silicon detector, fiber tracker, preshower detectors and calorimeter. Based on Ref. [5], a generic dE/dx cut is introduced with an efficiency of 68% for heavy stable charged particles and a rejection factor of 10 for the minimum ionization particles (MIP). Note that the efficiency for identifying at least one such particle in events with two heavy stable charged particles is 90%.

With the addition of preshower detectors, DØ will be able to reconstruct the distance of the closest approach (DCA) of a photon with a resolution ~ 1.5 cm [5]. Here the DCA is defined as the distance between the primary event vertex and the reconstructed photon direction. Thereby it will enable us to identify photons produced at secondary vertices. In the following, a photon is called displaced if its DCA is greater than 5.0 cm and is denoted by γ'. We further assume that the probability for a photon produced at the primary vertex to have the measured DCA> 5 cm is $\mathcal{P}(\gamma \to \gamma') = 2 \times 10^{-3}$ (about 3σ).

All final states studied have large E_T (p_T) leptons/photons with or without large $\not\!\!E_T$. Triggering on these events are not expected to have any problem. Nevertheless, we assume a 90% trigger efficiency for all the final states.

---

[*]The typical numbers determined in Run I are $\mathcal{P}(j \to e) = 5 \times 10^{-4}$, $\mathcal{P}(j \to \gamma) = 7 \times 10^{-4}$, and $\mathcal{P}(e \to \gamma) = 4 \times 10^{-3}$.

III. FINAL STATES

Signatures for supersymmetry vary dramatically from one model to another. They can also be very different for different regions of the parameter space in a model. Furthermore, these signatures are generally not unique to supersymmetry. In fact, some of the signatures are also expected from other theories beyond the Standard Model. Instead of chasing after theoretical models (all of which except perhaps one are wrong anyway) a set of final states which are somewhat generic to many new physics models, including supersymmetric models, is identified. All of these final states are characterized by high $E_T(p_T)$ isolated leptons/photons with or without large missing transverse momentum and are thus expected to have small physics and instrumental backgrounds. In the following, we discuss selection criteria and estimate observable background cross sections for six such final states:

$\gamma\gamma\not\!\!E_T$	di-photon events with large $\not\!\!E_T$
$\gamma bj\not\!\!E_T$	single-photon events with b-jets and large $\not\!\!E_T$
$\gamma' jj\not\!\!E_T$	single displaced photon events with jets and large $\not\!\!E_T$
$\ell\ell + dE/dx$	high p_T di-lepton events with large ionization energy
$\ell\ell\ell j\not\!\!E_T$	tri-lepton events with jets and $\not\!\!E_T$
$\ell^{\pm}\ell^{\pm} jj\not\!\!E_T$	like-sign di-lepton events with jets and $\not\!\!E_T$

A. $\gamma\gamma\not\!\!E_T$ Final State

The DØ Collaboration reported a search [7] for di-photon events with large $\not\!\!E_T$ ($\gamma\gamma\not\!\!E_T$ events) motivated by supersymmetric models with a light gravitino ($\tilde{G}$) as the LSP from a data sample of an integrated luminosity ($\mathcal{L}$) of 106.3 ± 5.6 pb^{-1} in Run I. The $\gamma\gamma\not\!\!E_T$ events were selected by requiring two identified photons, one with $E_T^{\gamma} > 20$ GeV and the other with $E_T^{\gamma} > 12$ GeV, each within pseudorapidity $|\eta^{\gamma}| < 1.1$ or $1.5 < |\eta^{\gamma}| < 2.0$, and a $\not\!\!E_T$ greater than 25 GeV. Two events satisfied all requirements.

The principal backgrounds were multijet, direct photon, $W + \gamma$, $W +$ jets, $Z \to ee$, and $Z \to \tau\tau \to ee$ events from Standard Model processes with misidentified photons and/or mismeasured $\not\!\!E_T$. The numbers of estimated background events were 2.1 ± 0.9 from $\not\!\!E_T$ mismeasurement (QCD) and 0.2 ± 0.1 from misidentified photons (fakes). This led to an observed background cross section of 20 fb from QCD and of 2 fb from fakes in Run I. The $\not\!\!E_T$ distributions before the $\not\!\!E_T$ cut for both candidates and background events are shown in Fig. 1. Note that events with large $\not\!\!E_T$ are rare.

Since the backgrounds are dominated by the $\not\!\!E_T$ mismeasurement, they can be significantly reduced by raising the $\not\!\!E_T$ cut. Therefore, the following selection criteria are used for the Run II studies:

1) At least two photons with $E_T^{\gamma} > 20$ GeV;

2) $\not\!\!E_T >$ 50 GeV.

The backgrounds with this set of selection criteria are expected to be significantly reduced by the increased cutoffs on $\not\!\!E_T$ and photon E_T and by the improved photon identification. The total observable background cross section in Run II is estimated to be $\sigma_b = 0.4(\text{QCD}) + 0.2(\text{fakes}) = 0.6$ fb assuming reduction factors of 5 from the raised $\not\!\!E_T$ cutoff, 4 from the improved $\mathcal{P}(j \to \gamma)$, 3 from the higher photon E_T requirement, and 10 from the decreased $e \to \gamma$ fake probability.

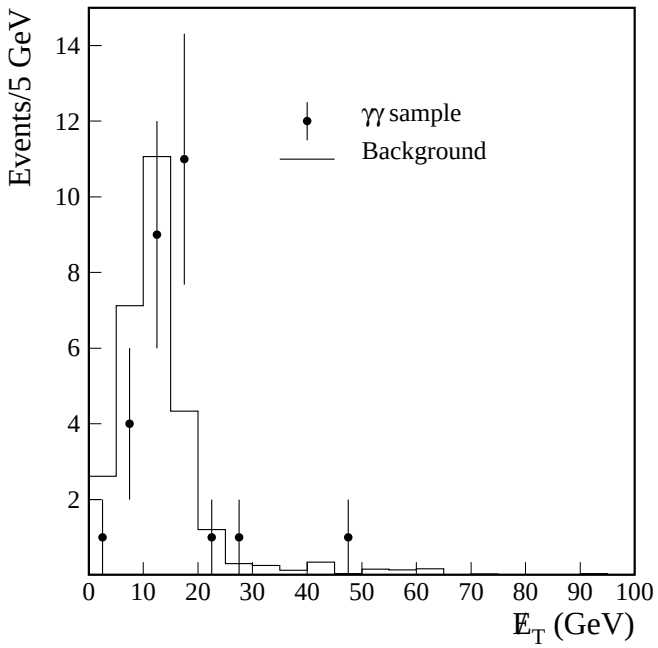

FIG. 1. The $\not\!\!E_T$ distributions of the $\gamma\gamma$ and background samples for Run I. The number of events with $\not\!\!E_T <$ 20 GeV in the background sample is normalized to that in the $\gamma\gamma$ sample. Note that there is a 14 GeV $\not\!\!E_T$ requirement in the trigger. The $\not\!\!E_T$ values plotted here are calculated off-line and therefore may differ from their values at the trigger level.

B. $\gamma bj\not\!\!E_T$ Final State

DØ Collaboration carried out a search [8] for single-photon events with at least two jets and large $\not\!\!E_T$ ($\gamma jj\not\!\!E_T$ events) in Run I. The $\gamma jj\not\!\!E_T$ events were selected by requiring at least one identified photon with $E_T^\gamma > 20$ GeV and within pseudorapidity ranges $|\eta^\gamma| < 1.1$ or $1.5 < |\eta^\gamma| < 2.0$, two or more jets having $E_T^j > 20$ GeV and $|\eta^j| < 2.0$, and $\not\!\!E_T > 25$ GeV. A total of 318 events were selected from a data sample corresponding to an integrated luminosity of 99.4 ± 5.4 pb^{-1}.

The principal backgrounds were found to be QCD direct photon and multijet events, where there was mismeasured $\not\!\!E_T$ and a real or fake photon. The number of events from this source was estimated to be 315 ± 30. Other backgrounds such as those from W with electrons misidentified as photons were found to be small, contributing 5 ± 1 events. This led to an observed background cross section of 3,200 fb from the $\not\!\!E_T$ mismeasurement and of 50 fb from the fakes. The $\not\!\!E_T$ distribution before the $\not\!\!E_T >$ 25 GeV cut is shown in Fig. 2. As

shown in the figure, the backgrounds can be significantly reduced by raising the requirement on $\not\!\!E_T$.

Events with a high E_T photon, b-jets and large $\not\!\!E_T$ are expected in some new physics models. These events, referred to as $\gamma bj\not\!\!E_T$, are in many ways similar to the $\gamma jj\not\!\!E_T$ events and thereby can be selected similarly:

1) At least one photon with $E_T^\gamma > 20$ GeV;

2) At least two jets with $E_T^j > 20$ GeV;

3) At least one jet is tagged as a b-quark jet with $E_T^b > 20$ GeV;

4) $\not\!\!E_T > 50$ GeV;

5) No leptons with $E_T^\ell > 20$ GeV.

The backgrounds from the QCD multijet events with real or misidentified photons and from the W events with electrons faking photons are estimated to be 0.63 fb, assuming background reduction factors of 5 from the raised $\not\!\!E_T$ requirement, 2 from the improved photon identification and using the assumed value of $\mathcal{P}(j \to b)$. The dominant background sources are expected to be $\gamma b\bar{b}$ and $\gamma t\bar{t}$ events. These background sources cannot be reduced by the tagging of b-jets. However, the $\gamma b\bar{b}$ contribution is expected to be small due to the large $\not\!\!E_T$ requirement. Monte Carlo studies show that it is negligible. The $\gamma t\bar{t}$ (with $t\bar{t} \to W^+W^-b\bar{b}$) contribution is reduced by the requirements 4) and 5) and is estimated using the cross section of Ref. [9]. A total of 0.9 fb observable background cross section is assumed.

C. $\gamma' jj\not\!\!E_T$ Final State

Photons produced at secondary vertices are predicted in a class of new physics models. These photons will appear to have large values of DCA. Though dramatic, they alone are unlikely to be sufficient to reduce backgrounds from cosmic rays or from mismeasurement. We therefore select events with displaced photons accompanied by jets and large $\not\!\!E_T$:

1) At least one displaced photon with $E_T^{\gamma'} > 20$ GeV;

2) At least two jets with $E_T^j > 20$ GeV;

3) $\not\!\!E_T > 50$ GeV.

These are called $\gamma' jj\not\!\!E_T$ events. The dominant backgrounds are the same as those for the $\gamma jj\not\!\!E_T$ events, with a vertex-pointing photon being misidentified as a displaced photon. Using $\mathcal{P}(\gamma \to \gamma')$, the observable background cross section from QCD and W events is estimated to be 0.6 fb.

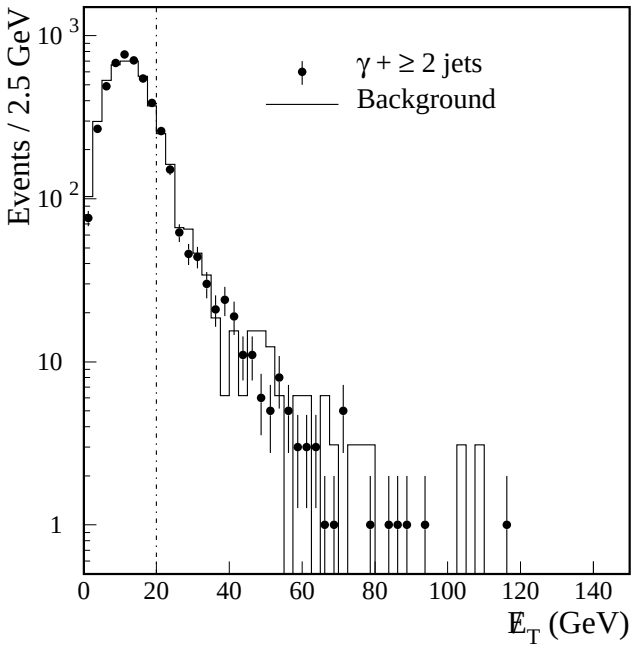

FIG. 2. The $\not\!\!E_T$ distributions of the γjj and background events. The number of events in the background is normalized to the γjj sample for $\not\!\!E_T < 20$ GeV, the region left of the dot-dashed line.

D. High p_T $\ell\ell + dE/dx$ Final State

One possible new physics signature is the presence of heavy stable charged particles. These particles, if produced, will manifest themself in the detector as slowly moving muons with large ionization energy losses. Though DØ had several di-lepton analyses in Run I, none of these can be extrapolated to Run II, thanks to the replacement of the central tracker. Based on the expected signatures of several supersymmetric models with heavy stable charged particles discussed below, we select high p_T di-lepton events ($\ell\ell + dE/dx$) with large dE/dx loss using the following requirements:

1) At least two leptons with $p_T^\ell > 50$ GeV;

2) $M_{\ell\ell} > 150$ GeV;

3) At least one lepton passing the dE/dx requirement.

The di-lepton mass requirement is intended to reduce Drell-Yan backgrounds. The principal backgrounds are: QCD dijet events with jets misidentified as leptons, $t\bar{t}$, and Drell-Yan events. Using $\mathcal{P}(j \to \ell) = 10^{-4}$ and the assumed rejection factor of the dE/dx cut for the MIP particles, the observable background cross sections are estimated to be 0.1 fb from QCD dijet, 0.2 fb from $t\bar{t}$ events, and 0.2 fb from Drell-Yan processes. The QCD dijet cross section for $p_T > 50$ GeV is assumed to be 1 μb in the estimation. The total observable cross section is therefore 0.5 fb for the above selection.

E. $\ell\ell\ell j \not\!\!E_T$ Final State

DØ searched for gaugino pair production using the tri-lepton signature [10] in Run I. The lepton p_T cut was typically 15 GeV for the leading lepton and 5 GeV for the non-leading leptons. The analysis also had a small $\not\!\!E_T$ requirement. The observable background cross section was estimated to be around 13 fb. Most of these backgrounds are due to Drell-Yan processes. We select the $\ell\ell\ell j \not\!\!E_T$ events using the following criteria:

1) $p_T^{\ell_1} > 15$ GeV, $p_T^{\ell_2} > 5$ GeV, $p_T^{\ell_3} > 5$ GeV;

2) $\not\!\!E_T > 20$ GeV;

3) At least one jet with $E_T^j > 20$ GeV.

The Drell-Yan production, a major background source for the Run I analysis, is significantly reduced by the new jet requirement. The total observable background cross section is estimated to be 0.3 fb assuming background reduction factors of 10 from the jet requirement, 2 from the improved particle identification, 2 from the higher $\not\!\!E_T$ cut.

F. $\ell^\pm\ell^\pm jj \not\!\!E_T$ Final State

Like-sign di-lepton events are expected from processes such as gluino pair production. They are also expected from processes with three or more leptons in the final states, but only two are identified. This final state is expected to have small backgrounds. Again without a magnetic tracker, DØ had no analysis of this nature in Run I. Based on Monte Carlo studies for several supersymmetric models, we select $\ell^\pm\ell^\pm jj \not\!\!E_T$ events using the following criteria:

1) Two like-sign leptons with $p_T^\ell > 15$ GeV;

2) At least two jets with $E_T^j > 20$ GeV;

3) $\not\!\!E_T > 25$ GeV.

Events with three or more identified leptons are removed to make the sample orthogonal to the $\ell\ell\ell j \not\!\!E_T$ sample. Since leptons are relatively soft in p_T for the new physics model we investigated using this selection, the effect of charge confusion due to a limited tracking resolution is thus neglected in this study. The major backgrounds are: W + jets events with one of the jets misidentified as a lepton, $t\bar{t}$ events with energetic leptons from b-quark decays, and Drell-Yan (WZ, ZZ) events. The W + jets background is estimated using the number of $W + 3j$ events observed in Run I folded with $\mathcal{P}(j \to \ell)$ to be 0.2 fb. The $t\bar{t}$ and Drell-Yan backgrounds are estimated using Monte Carlo to be 0.1 and 0.1 fb respectively. Adding the three background sources together yields a total observable background cross section of 0.4 fb.

IV. CONSTRAINTS ON GMSB MODELS

The supersymmetric models with gauge mediated supersymmetry breaking are characterized by a supersymmetry breaking scale Λ as low as 100 TeV and a light gravitino which is naturally the lightest supersymmetric particle. In these models, supersymmetry is assumed to be broken in a hidden sector and the symmetry breaking is transmitted to the visible sector of Standard Model particles and their superpartners through the Standard Model gauge interactions. The minimum gauge mediated supersymmetry breaking model is described by five parameters:

Λ:	supersymmetry breaking scale
M_m:	messenger sector scale
N:	number of messengers
$\tan\beta$:	ratio of the v.e.v of the two higgs doublets
sign(μ):	sign of the higgs mass parameter

The phenomenology is largely determined by the next-to-lightest supersymmetric particle which in turn depends on the values of the above five parameters. For a review of GMSB models, see Ref. [2]. In the following, we discuss expected sensitivities with integrated luminosities of 2, 30 fb^{-1} for four different model lines defined by the working group. Each model line has a different NLSP. All theoretical expectations and signal efficiencies are obtained from the ISAJET MC program. A minimum p_T of 50 GeV of the hard scattering is applied for all signal processes. We define the significance ($N_s/\delta N_b$) as the ratio between the number (N_s) of expected signal events and the error (δN_b) on the estimated number of background events. Here a 20% systematic uncertainty is assumed for all estimated observable background cross sections. Therefore,

$$\delta N_b = \sqrt{\mathcal{L}\cdot\sigma_b + (0.2\cdot\mathcal{L}\cdot\sigma_b)^2}$$

We characterize the sensitivity using the minimum signal cross section σ_{dis} for a 5 standard deviation (5σ) discovery:

$$\frac{N_s}{\delta N_b} = \frac{\mathcal{L}\cdot\sigma_{dis}\cdot\epsilon}{\delta N_b} = 5$$

where ϵ is the efficiency for the signal. The minimum observable signal cross section σ_{obs} defined as $\sigma_{dis}\cdot\epsilon$ for the discovery is therefore independent of signal processes. The σ_{obs} as a function of $\mathcal{L}$ for several different values of σ_b are shown in Fig. 3. It decreases dramatically as $\mathcal{L}$ increases for small $\mathcal{L}$ values and flattens out for large $\mathcal{L}$ values. Clearly, the sensitivity can be improved for large $\mathcal{L}$ values by tightening the cuts to reduce backgrounds further.

In the following, we express the 5σ discovery cross sections as functions of the supersymmetry breaking scale Λ and the lighter chargino ($\tilde{\chi}_1^{\pm}$) mass for the four different model lines.

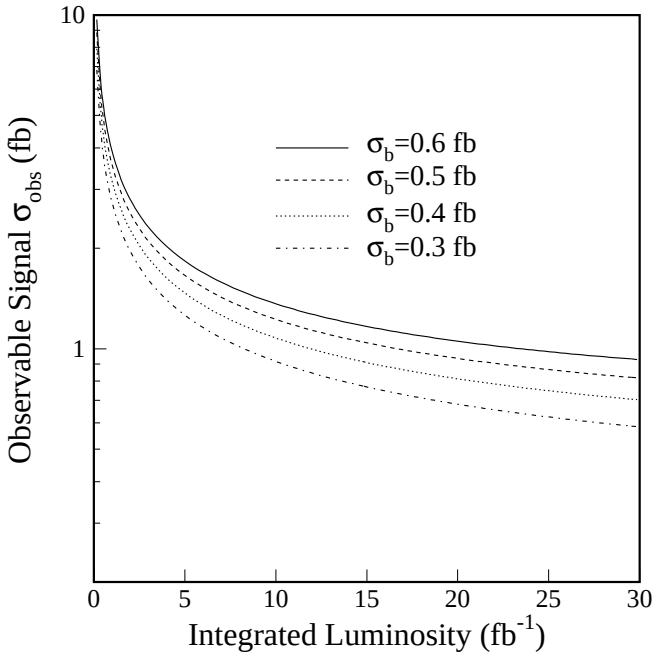

FIG. 3. The minimum observable signal cross section σ_{obs} for a 5σ discovery as a function of integrated luminosity for four different values of background cross sections.

A. Model Line 1: $\tilde{\chi}_1^0$ as the NLSP

Within the framework of the minimal GMSB models, $\tilde{\chi}_1^0$ is the NLSP for most of the parameter space. If the $\tilde{\chi}_1^0$ has a non-zero photino component, it is unstable and decays to a photon plus a gravitino ($\tilde{\chi}_1^0 \rightarrow \gamma\tilde{G}$) with a branching ratio of nearly 100%. Depending on its lifetime, pair production of supersymmetric particles will result in $\gamma\gamma \not\!\!E_T$, $\gamma \not\!\!E_T$, and $\not\!\!E_T$+X events. For the purpose of this study, we consider a class of models with the following parameters fixed:

$$N = 1, \quad \frac{M_m}{\Lambda} = 2, \quad \tan\beta = 2.5, \quad \mu > 0$$

while Λ is allowed to vary. For the range of Λ values of interest at the Tevatron, the supersymmetry production cross section is dominated by $\tilde{\chi}_1^{\pm}\tilde{\chi}_1^{\pm}$ and $\tilde{\chi}_1^{\pm}\tilde{\chi}_2^0$ production. Figure 4 shows the schematic decay chains of $\tilde{\chi}_1^{\pm}$ and $\tilde{\chi}_2^0$ with their branching ratios for $\Lambda = 100$ TeV. In the following, scenarios with prompt and delayed $\tilde{\chi}_1^0$ decays are discussed. If the $\tilde{\chi}_1^0$ is quasi-stable, *i.e.* with a long lifetime, the signature will be identical to that of the supersymmetric models with gravity mediation.

1. Prompt $\tilde{\chi}_1^0 \rightarrow \gamma\tilde{G}$ Decay

If the $\tilde{\chi}_1^0$ decays in the vicinity of the production vertex, $\gamma\gamma \not\!\!E_T$ events are expected. The distributions of photon E_T and event $\not\!\!E_T$ for $\Lambda = 80, 140$ TeV are shown in Fig. 5. These events typically have high E_T photons together with large transverse momentum imbalances, and therefore can be selected using the $\gamma\gamma \not\!\!E_T$ criteria discussed in Section III A. Table I shows the detection efficiencies, significances along with the total theoretical cross

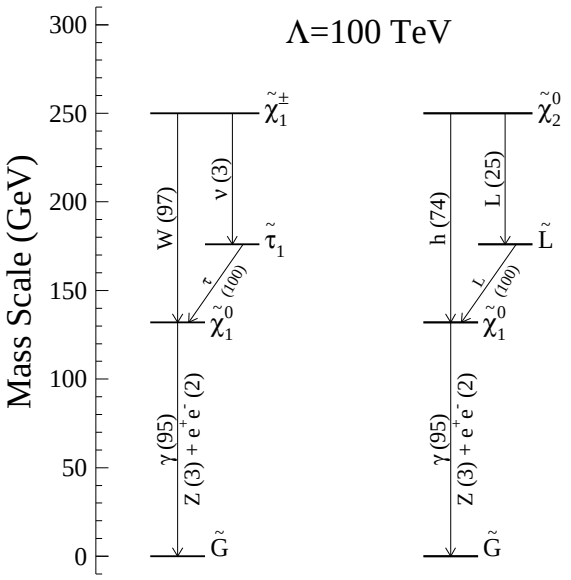

FIG. 4. Decay schematics of $\tilde{\chi}_1^{\pm}$ and $\tilde{\chi}_2^0$ for $\Lambda = 100$ TeV for the model line with a $\tilde{\chi}_1^0$ as the NLSP. Percentage branching ratios for main decay modes are shown in parentheses.

sections of supersymmetry, chargino and neutralino masses for different values of Λ. Figure 6 compares the 5σ discovery cross sections σ_{dis} with the theoretical cross sections expected from supersymmetry for two different values of $\mathcal{L}$ as functions of the lighter chargino mass $m_{\tilde{\chi}_1^{\pm}}$ (and the supersymmetry breaking scale Λ). The lighter chargino with mass up to 290, 340 GeV can be discovered for $\mathcal{L}$=2, 30 fb^{-1} respectively.

Λ (TeV)	60	80	100	120	140	160
σ_{th} (fb)	464	105	27	7.7	2.2	0.7
$m_{\tilde{\chi}_1^{\pm}}$ (GeV)	138	194	249	304	357	410
$m_{\tilde{\chi}_1^0}$ (GeV)	75	104	132	160	188	216
ϵ (%)	16.1	24.3	28.2	30.1	30.6	30.2
$N_s/\delta N_b$ (2 fb^{-1})	136	46	14	4.2	1.2	0.4
$N_s/\delta N_b$ (30 fb^{-1})	400	137	41	12	3.6	1.1

TABLE I. The supersymmetry cross section (σ_{th}), $\tilde{\chi}_1^{\pm}$ and $\tilde{\chi}_1^0$ masses, detection efficiency of the $\gamma\gamma\not{E}_T$ selection, and significances for different values of Λ for the models with a short-lived $\tilde{\chi}_1^0$ as the NLSP (model line 1). The relative statistical error on the efficiency is typically 2%. The observable background cross section is assumed to be 0.6 fb with a 20% systematic uncertainty.

2. Delayed $\tilde{\chi}_1^0 \to \gamma\tilde{G}$ Decay

If the $\tilde{\chi}_1^0$ has a significant lifetime, the photon from its decay may not point back to the primary vertex. If the decay occurs inside the tracking volume of the DØ detector, the

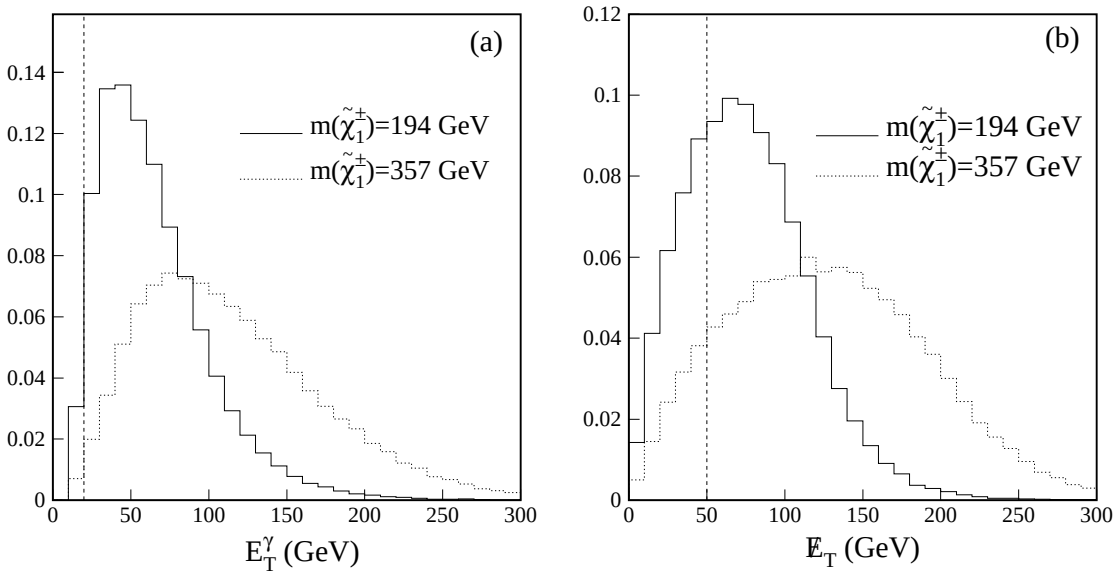

FIG. 5. Distributions of (a) photon E_T and (b) event $\not\!\!E_T$ for Λ = 80, 140 TeV ($m_{\tilde{\chi}_1^{\pm}}$ = 194, 357 GeV) for the models with a short-lived $\tilde{\chi}_1^0$ as the NLSP. The vertical dashed lines indicate the cutoffs. All distributions are normalized to have unit area.

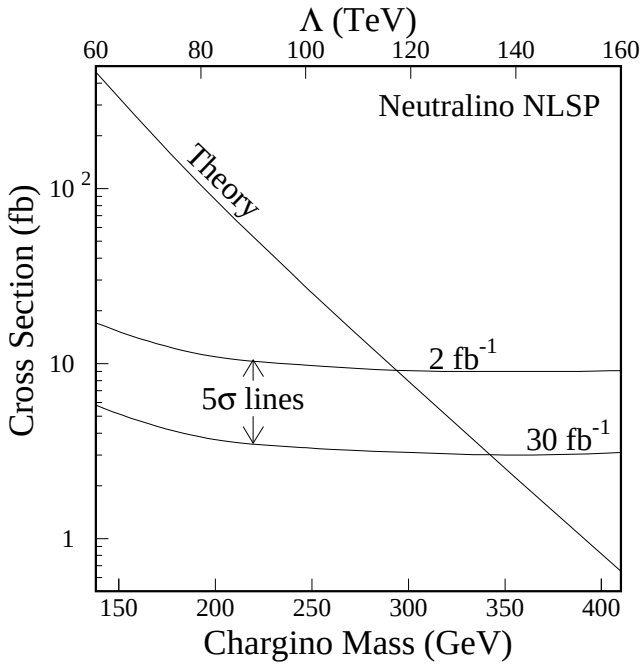

FIG. 6. The 5σ discovery cross section curves as functions of mass of the lighter chargino (and the supersymmetry breaking scale Λ) along with the theoretical cross sections for the model line 1. The NLSP $\tilde{\chi}_1^0$ is assumed to be short-lived. Two curves corresponding to integrated luminosities of 2 and 30 fb^{-1} are shown.

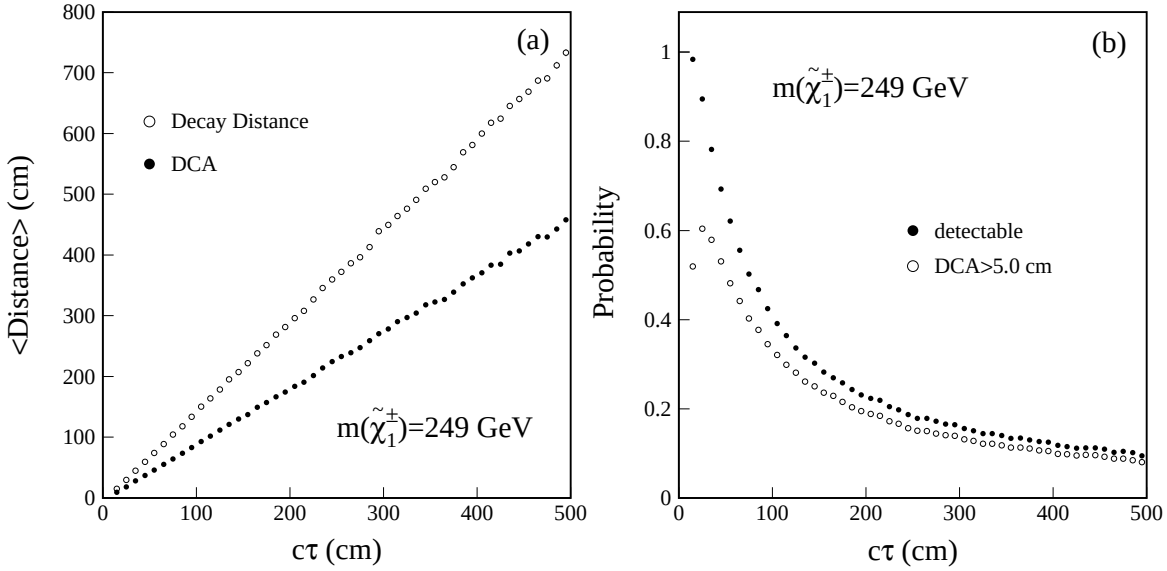

FIG. 7. (a) Average decay distance and DCA for different values of proper decay distance $c\tau$ of the NLSP $\tilde{\chi}_1^0$. (b) The probability that a photon decays within the tracking volume and the probability that such a photon has its DCA$>$ 5 cm as functions of $c\tau$. Note that $\Lambda = 100$ TeV ($m_{\tilde{\chi}_1^{\pm}} = 249$ GeV) for both plots.

photon is expected to traverse standard electromagnetic detectors (the preshower detectors and the electromagnetic calorimeter). It, therefore, can be identified. However, if the decay occurs outside the tracking detector, the photon identification is problematic. For this study, we assume that the photon is identifiable if it is produced inside a cylinder defined by the DØ tracking volume ($r < 50$ cm and $|z| < 120$ cm) and is lost if it is produced outside the cylinder. Figure 7(a) shows the average decay distance and distance of closest approach of the $\tilde{\chi}_1^0$ as functions of its proper decay length (cτ) for $\Lambda = 100$ TeV. Due to its heavy mass, the Lorentz boost for the $\tilde{\chi}_1^0$ is typically small ($\gamma \sim 1.5$). The probabilities that a photon is identifiable and that an identifiable photon has DCA$>$ 5 cm as functions of the $\tilde{\chi}_1^0$ proper decay distance $c\tau$ are shown in Fig. 7(b), again for $\Lambda = 100$ TeV. Distributions for other Λ values are similar. Figure 8 shows jet multiplicity and E_T distributions for $\Lambda = 80,\ 140$ TeV. Most of these events have large E_T jets and thus can be selected using the $\gamma' jj\not{E}_T$ selection criteria discussed above. The detection efficiencies and the expected significances of the $\gamma' jj\not{E}_T$ selection for $c\tau = 50$ cm are tabulated in Table II as an example. The estimated 5σ discovery reaches in Λ and chargino mass for different values of $c\tau$ are shown in Fig. 9 along with those expected from the $\gamma\gamma\not{E}_T$ analysis. As expected, the $\gamma\gamma\not{E}_T$ analysis has a stronger dependence on $c\tau$ than the $\gamma' jj\not{E}_T$ analysis.

B. Model Line 2: $\tilde{\tau}_1$ as the NLSP

If $\tilde{\tau}_1$ (the lighter of the two mixed states of $\tilde{\tau}_R$ and $\tilde{\tau}_L$) is lighter than $\tilde{\chi}_1^0$, all supersymmetric particles will cascade into the $\tilde{\tau}_1$ which in turn will decay to $\tau\tilde{G}$ with a 100%

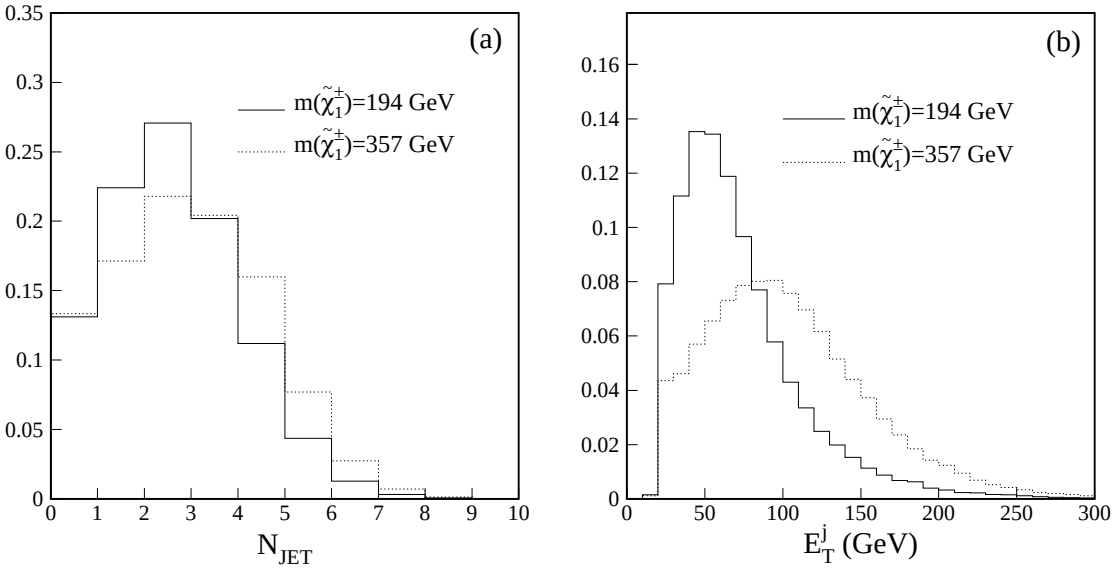

FIG. 8. Distributions of (a) jet multiplicity and (b) jet E_T for Λ = 80, 140 TeV ($m_{\tilde{\chi}_1^{\pm}}$ = 194, 357 GeV) for the models with $\tilde{\chi}_1^0$ as the NLSP. All distributions are normalized to have unit area.

Λ (TeV)	60	80	100	120	140	160
σ_{th} (fb)	464	105	27	7.7	2.2	0.7
$m_{\tilde{\chi}_1^{\pm}}$ (GeV)	138	194	249	304	357	410
$m_{\tilde{\chi}_1^0}$ (GeV)	75	104	132	160	188	216
ϵ (%)	11.2	23.6	31.1	33.3	33.2	32.1
$N_s/\delta N_b$ (2 fb^{-1})	93	44	15	4.6	1.3	0.4
$N_s/\delta N_b$ (30 fb^{-1})	278	133	45	14	3.9	1.2

TABLE II. The detection efficiency of the $\gamma' jj\not{E}_T$ selection, and the significances for different values of Λ for the models with $\tilde{\chi}_1^0$ as the NLSP. The $\tilde{\chi}_1^0$ proper decay distance $c\tau$ is assumed to be 50 cm. The relative statistical error on the efficiency is typically 2%. The observable background cross section is assumed to be 0.6 fb with a 20% systematic uncertainty.

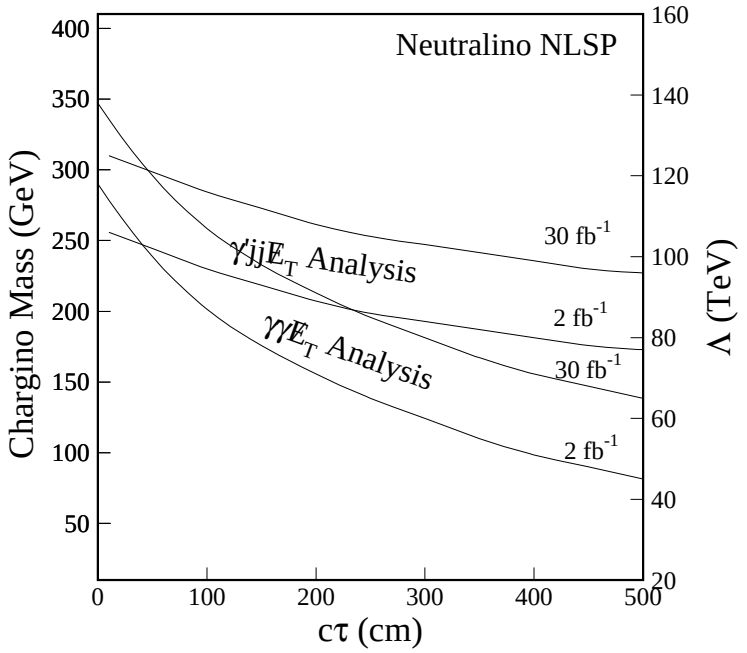

FIG. 9. The 5σ discovery reaches of the $\gamma' jj\not{E}_T$ and the $\gamma\gamma\not{E}_T$ analyses in $m_{\tilde{\chi}_1^\pm}$ and Λ as functions of the proper decay distance of the $\tilde{\chi}_1^0$ NLSP for $\mathcal{L}$=2, 30 fb^{-1}.

branching ratio. This class of models is defined by following parameter values:

$$N = 2, \quad \frac{M_m}{\Lambda} = 3, \quad \tan\beta = 15, \quad \mu > 0$$

with varying Λ. Again, $\tilde{\chi}_1^\pm\tilde{\chi}_1^\pm$ and $\tilde{\chi}_1^\pm\tilde{\chi}_2^0$ dominate the production cross section for $\Lambda \lesssim$ 75 TeV. For Λ values above 75 TeV, $\tilde{\tau}_1\tilde{\tau}_1$, $\tilde{e}_R\tilde{e}_R$, and $\tilde{\mu}_R\tilde{\mu}_R$ productions become important. As an example, branching ratios of $\tilde{\chi}_1^\pm$ and $\tilde{\chi}_2^0$ for $\Lambda = 40$ TeV are graphically displayed in Fig. 10. In the following, two cases corresponding to short-lived and quasi-stable $\tilde{\tau}_1$s are discussed. It should be noted that the two analyses discussed below are also sensitive to the case with a intermediate $\tilde{\tau}_1$ lifetime.

1. Prompt $\tilde{\tau}_1 \to \tau\tilde{G}$ Decay

If the $\tilde{\tau}_1$ is short-lived and decays in the vicinity of the production vertex (*i.e.* with a decay distance $\gamma c\tau \lesssim 10$ cm), anomalous τ production is expected from supersymmetry. Together with the W^*/Z^* productions from the cascade decays of primary supersymmetric particles, these events will give rise to $\ell\ell\ell j\not{E}_T$ and $\ell^\pm\ell^\pm jj\not{E}_T$ final states. The lepton p_T distributions of the $\ell\ell\ell j\not{E}_T$ and $\ell^\pm\ell^\pm jj\not{E}_T$ events are shown in Fig. 11. Since most leptons are produced in τ decays, their p_Ts are relatively soft. Table III shows the efficiencies of the $\ell\ell\ell j\not{E}_T$ and $\ell^\pm\ell^\pm jj\not{E}_T$ selection criteria for these events along with the theoretical cross sections, $\tilde{\chi}_1^\pm$ and $\tilde{\tau}_1$ masses. Note that the $\ell\ell\ell j\not{E}_T$ and $\ell^\pm\ell^\pm jj\not{E}_T$ criteria are orthogonal. The efficiencies are relatively small largely due to the small branching ratio of the events to tri-leptons. We note that the total efficiencies shown in the table are somewhat conservative.

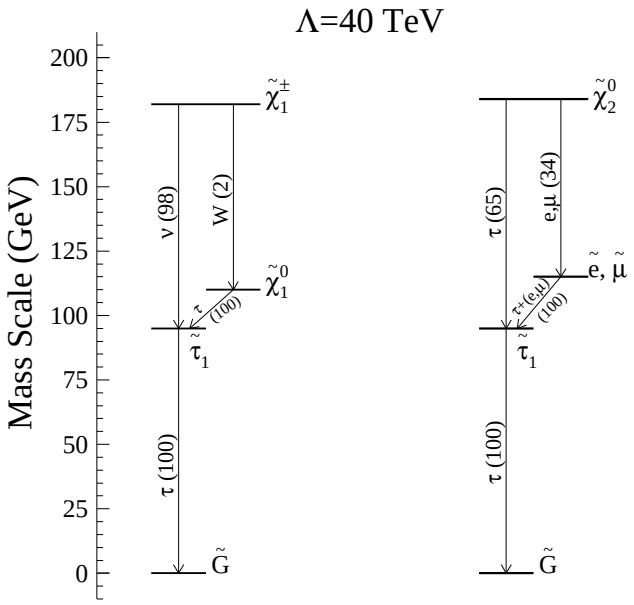

FIG. 10. Decay schematics of $\tilde{\chi}_1^{\pm}$ and $\tilde{\chi}_2^0$ for $\Lambda = 40$ TeV for the model line with a $\tilde{\tau}_1$ as the NLSP. Percentage branching ratios for main decay modes are shown in parentheses.

They do not take into account the migration of the $\ell\ell\ell j \not{E}_T$ events to the $\ell^{\pm}\ell^{\pm} jj \not{E}_T$ events due to inefficiency in the lepton identification. The 5σ discovery curves are shown in Fig. 12. The lighter chargino with mass up to 160 and 230 GeV can be discovered for $\mathcal{L}$=2, 30 fb^{-1}.

The conventional wisdom is that this analysis should benefit from a τ identification. However, we doubt that it will have a dramatic impact on the reach in the supersymmetry parameter space. Though a τ identification could improve the efficiency for the signal, it will undoubtably come with large backgrounds. Nevertheless, a τ identification is essential to narrow down theoretical models if an excess is observed in the tri-lepton final state.

2. Quasi-stable $\tilde{\tau}_1$

If the $\tilde{\tau}_1$ has a long lifetime (quasi-stable) and decays outside the detector ($\gamma c\tau$ greater than $\sim$ 3 m), it will appear in the detector like a muon with the exception of a large ionization energy loss. The signature is, therefore, two high p_T 'muons' with large dE/dx values. These events can be selected using the criteria described in Section III D. The expected p_T distributions of the $\tilde{\tau}_1$ for two different values of Λ are shown in Fig. 13(a). The cut of $p_T > 50$ GeV of the $\ell\ell + dE/dx$ selection is efficient for the signal while it is expected to reduce backgrounds significantly. The typical invariant mass of the two 'muons' (assuming massless) is very large as shown in Fig. 13(b). A $M_{\ell\ell} > 150$ GeV requirement does little harm to the signals. Due to its large mass, the $\tilde{\tau}_1$ is expected to move slowly. However since most of the $\tilde{\tau}_1$'s are produced in the decays of massive $\tilde{\chi}_1^{\pm}$s and $\tilde{\chi}_2^0$s, the average speed $\beta(\equiv v/c)$ is relatively large. It is around 0.7 for the Λ values studied. Note that the β distribution is very similar to that shown in Fig. 18(b) for the models with $\tilde{\ell}$ as the Co-NLSP.

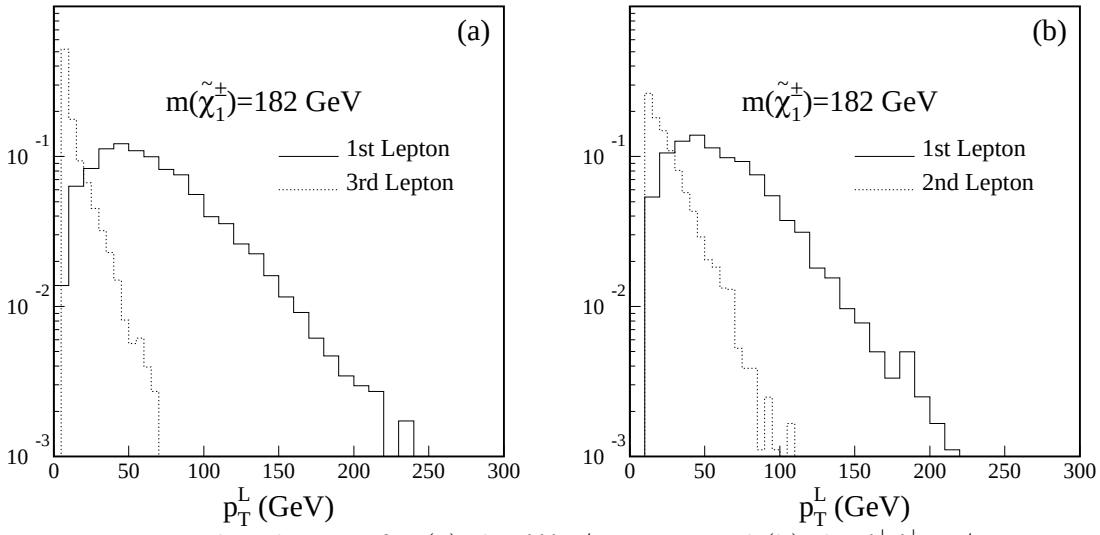

FIG. 11. Lepton p_T distributions for (a) the $\ell\ell\ell j\not{E}_T$ events and (b) the $\ell^{\pm}\ell^{\pm}jj\not{E}_T$ events of the models with a short-lived $\tilde{\tau}_1$ for $m_{\tilde{\chi}_1^{\pm}} = 182$ GeV ($\Lambda = 40$ TeV). All distributions are normalized to unit area.

Λ (TeV)	20	40	60	80
σ_{th} (fb)	5800	149	14.4	2.1
$m_{\tilde{\chi}_1^{\pm}}$ (GeV)	72	182	289	394
$m_{\tilde{\tau}_1}$ (GeV)	54	99	147	196
$\ell^{\pm}\ell^{\pm}jj\not{E}_T$ ϵ (%)	–	0.6	1.0	1.3
$\ell\ell\ell j\not{E}_T$ ϵ (%)	0.5	1.0	1.6	2.0
Total ϵ (%)	0.5	1.6	2.6	3.3
$N_s/\delta N_b$ (2 fb^{-1})	48	4.0	0.6	0.1
$N_s/\delta N_b$ (30 fb^{-1})	140	12	1.8	0.3

TABLE III. The theoretical cross section, $\tilde{\chi}_1^{\pm}$ and $\tilde{\tau}_1$ masses, detection efficiency of $\ell^{\pm}\ell^{\pm}jj\not{E}_T$ and $\ell\ell\ell j\not{E}_T$ selections, and significances for different values of Λ for the models with a short-lived $\tilde{\tau}_1$ as the NLSP. The relative statistical error on the efficiency is typically 25%. The combined $\ell^{\pm}\ell^{\pm}jj\not{E}_T$ and $\ell\ell\ell j\not{E}_T$ background cross section is assumed to be 0.7 fb with a 20% systematic uncertainty.

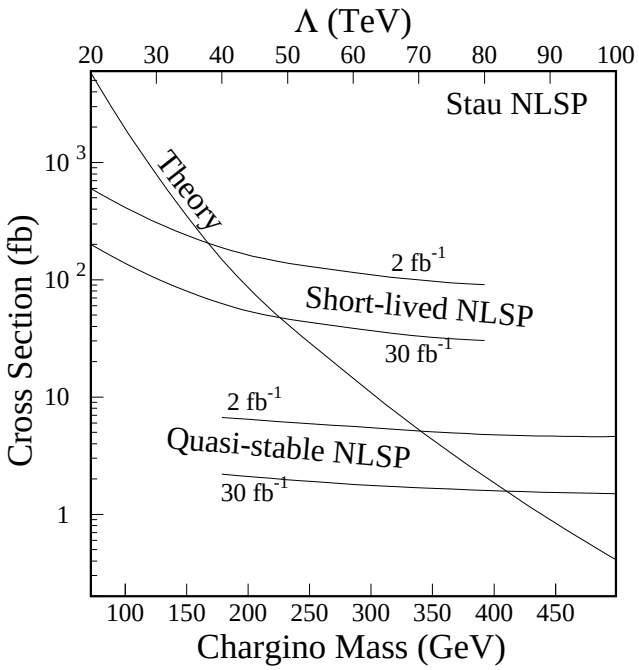

FIG. 12. The 5σ discovery cross section curves as functions of mass of the lighter chargino and the supersymmetry breaking scale Λ for the model line 2 along with the theoretical cross sections. The 5σ curves are shown for both short-lived and quasi-stable NLSP's and for integrated luminosities of 2, 30 fb^{-1}.

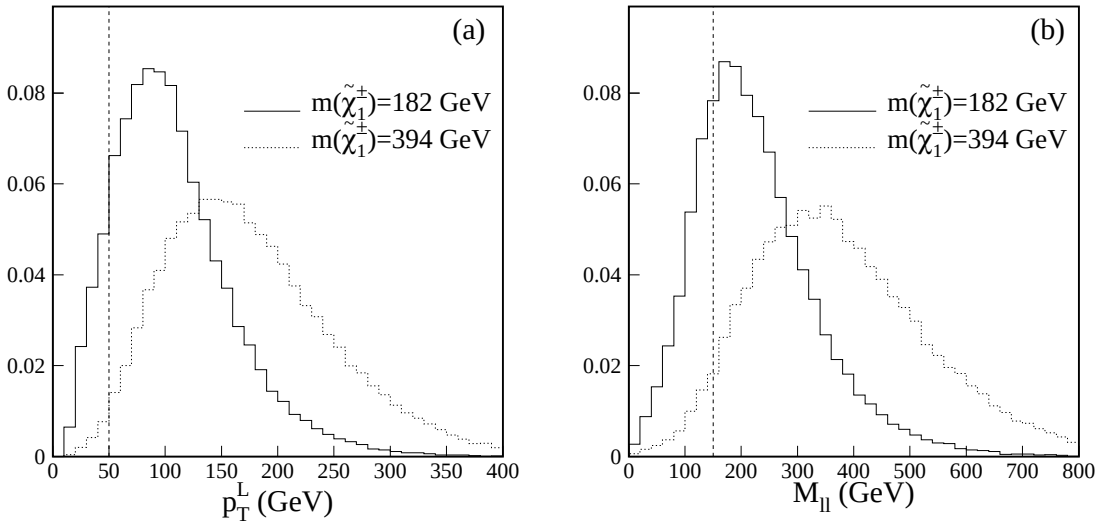

FIG. 13. The lepton p_T (a) and di-lepton mass $M_{\ell\ell}$ (b) distributions for the models with a quasi-stable $\tilde{\tau}_1$ as the NLSP for $\Lambda = 40,\ 80$ TeV ($m_{\tilde{\chi}_1^\pm} = 182,\ 394$ GeV). The vertical dashed lines indicate the cutoffs. All distributions are normalized to unit area.

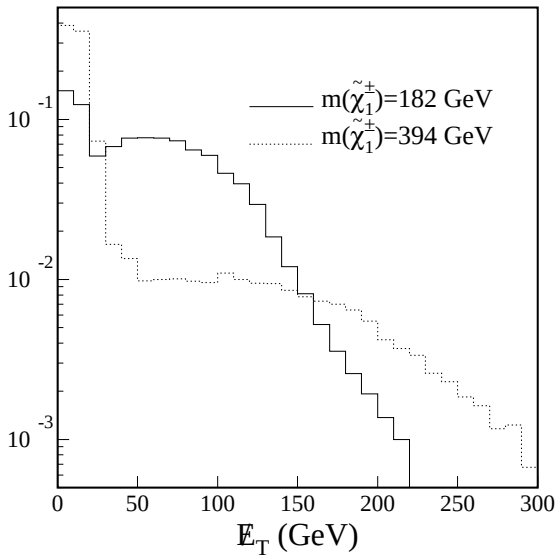

FIG. 14. The $\not\!\!E_T$ distributions for the models with a quasi-stable $\tilde{\tau}_1$ as the NLSP for $\Lambda = 40,\ 80$ TeV ($m_{\tilde{\chi}_1^{\pm}} = 182,\ 394$ GeV). The decays $\tilde{\chi}_1^{\pm} \to \tilde{\chi}_1^0 W^{\pm} \to \tilde{\tau}_1 \tau W^{\pm}$ and $\tilde{\chi}_2^0 \to e\tilde{e},\ \mu\tilde{\mu}$ contribute to events with small $\not\!\!E_T$ while the decays $\tilde{\chi}_1^{\pm} \to \tilde{\tau}_1 \nu$ and $\tilde{\chi}_2^0 \to \tau\tilde{\tau}_1$ are the source for events with large $\not\!\!E_T$.

Nevertheless, the not-so-slow moving $\tilde{\tau}_1$'s are expected to deposit large ionization energies in the detector, differentiating them from other high p_T MIP particles. Since the backgrounds for the requirements $p_T > 50$ GeV and $M_{\ell\ell} > 150$ GeV are already small, it pays to have a dE/dx requirement with a relatively high efficiency for the signal and a resonable rejection for the MIP particles. The $\not\!\!E_T$ distribution of these events as shown in Fig. 14 shows two distinct regions: small and large $\not\!\!E_T$. The decays $\tilde{\chi}_1^{\pm} \to \tilde{\chi}_1^0 W \to \tilde{\tau}_1 \tau W$ and $\tilde{\chi}_2^0 \to e\tilde{e},\ \mu\tilde{\mu}$ contribute to events with small $\not\!\!E_T$. The decays $\tilde{\chi}_1^{\pm} \to \tilde{\tau}_1 \nu$ and $\tilde{\chi}_2^0 \to \tau\tilde{\tau}_1$ are responsible for events with large $\not\!\!E_T$. The detection efficiencies and the expected significances of the $\ell\ell + dE/dx$ selection for different values of Λ are tabulated in Table IV. The high efficiency is largely due to the high momentum expected for the quasi-stable $\tilde{\tau}_1$. The 5σ discovery curves are shown in Fig. 12 for two values of $\mathcal{L}$. The lighter chargino with mass up to 340, 410 GeV and the $\tilde{\tau}_1$ with mass up to 160, 200 GeV can be discovered for the two integrated luminosities respectively.

C. Model Line 3: $\tilde{\ell}$ as the Co-NLSP

For some regions of the parameter space, three light sleptons ($\tilde{e}_R$, $\tilde{\mu}_R$, and $\tilde{\tau}_1$) are essentially degenerate in mass and they can be lighter than $\tilde{\chi}_1^0$. As a result, the sleptons ($\tilde{\ell} \equiv \tilde{\tau}_1, \tilde{e}_R, \tilde{\mu}_R$) effectively share the role of the NLSP. Quantitative studies of this type of models are done for following GMSB parameter values:

$$N = 3, \quad \frac{M_m}{\Lambda} = 3, \quad \tan\beta = 3, \quad \mu > 0$$

Λ (TeV)	40	60	80	100
σ_{th} (fb)	149	14.4	2.1	0.4
$m_{\tilde{\chi}_1^\pm}$ (GeV)	182	289	394	499
$m_{\tilde{\tau}_1}$ (GeV)	99	147	196	246
ϵ (%)	37.4	44.6	51.6	54.9
$N_s/\delta N_b$ (2 fb^{-1})	112	12	2.1	0.5
$N_s/\delta N_b$ (30 fb^{-1})	341	40	6.7	1.4

TABLE IV. The theoretical cross section, $\tilde{\chi}_1^\pm$ and $\tilde{\tau}_1$ masses, detection efficiency of the $\ell\ell$+dE/dx selection, and significances for different values of Λ for the models with a quasi-stable $\tilde{\tau}_1$ NLSP. The relative statistical error on the efficiency is typically 1%. The background cross section is assumed to be 0.5 fb with an uncertainty of 20%.

with again varying Λ values. For small values of Λ, $\tilde{\chi}_1^\pm\tilde{\chi}_1^\pm$ and $\tilde{\chi}_1^\pm\tilde{\chi}_2^0$ dominate the production cross section. As shown in Fig. 15, $\tilde{\chi}_1^\pm\tilde{\chi}_1^\pm$ and $\tilde{\chi}_1^\pm\tilde{\chi}_2^0$ production will yield events with multileptons in the final state. The slepton pair production surpasses chargino-neutralino production if $\Lambda \gtrsim 50$ TeV. The total supersymmetry cross section for several different Λ values can be found in Table V. The lifetime of $\tilde{\ell}$ determines the event topology. In the following, we discuss the cases with short-lived and quasi-stable $\tilde{\ell}$s. Again, the analyses should also be sensitive to the $\tilde{\ell}$ NLSP with a intermediate lifetime.

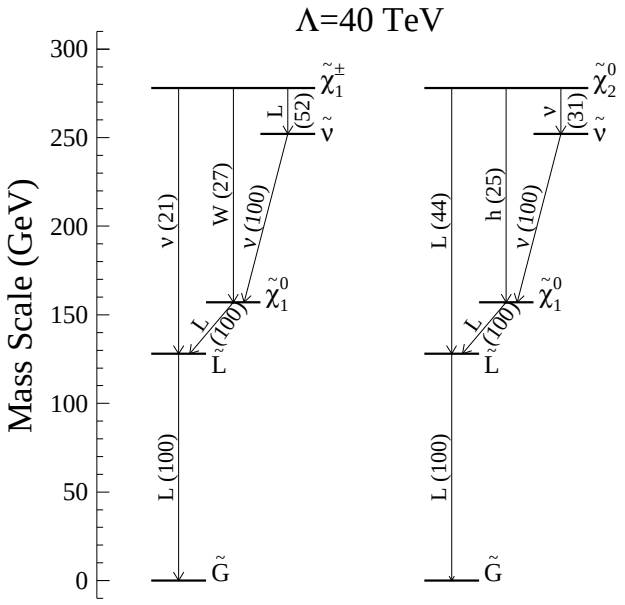

FIG. 15. Decay schematics of $\tilde{\chi}_1^\pm$ and $\tilde{\chi}_2^0$ for $\Lambda = 40$ TeV for the model line with scalar leptons as the Co-NLSP. Percentage branching ratios for main decay modes are shown in parentheses.

1. Prompt $\tilde{\ell} \to \ell\tilde{G}$ Decay

If the decay $\tilde{\ell} \to \ell\tilde{G}$ is prompt ($\gamma c\tau \lesssim 10$ cm), $\ell\ell\not{E}_T$ events are expected from supersymmetry. Unfortunately, this final state is swamped by backgrounds from the Standard Model processes such as $t\bar{t}$, WW, WZ and ZZ productions as well as from W + jets production with one of the jets misidentified as a lepton. However we note that these events typically have multiple leptons in the final state and most of them are in the central pseudorapidity region with good lepton identification. Apart from those from $\tilde{\ell}$ decays, leptons are also expected from W^*'s and Z^*'s produced in the cascade decays of $\tilde{\chi}_1^\pm$ and $\tilde{\chi}_2^0$ of supersymmetry originated events. Therefore, they can be selected using the $\ell\ell\ell j\not{E}_T$ criteria. The p_T distributions of the leading lepton and the third lepton of these events are shown in Fig. 16(a). Since most of the leading leptons are produced in the direct decays of heavy $\tilde{\ell}$'s, its p_T spectrum is relatively hard as shown in the figure. The detection efficiencies and the expected significances are summarized in Table V. The reduction in the relative cross section of the tri-lepton producing $\tilde{\chi}_1^\pm\tilde{\chi}_1^\pm$ and $\tilde{\chi}_1^\pm\tilde{\chi}_2^0$ processes is responsible for the decrease in efficiency as Λ increases. For $\Lambda \gtrsim 50$ TeV, the $\tilde{\ell}\tilde{\ell}$ production cross section surpasses that of the $\tilde{\chi}_1^\pm\tilde{\chi}_1^\pm$ and $\tilde{\chi}_1^\pm\tilde{\chi}_2^0$. With the $\tilde{\ell} \to \ell\tilde{G}$ decay, $\tilde{\ell}\tilde{\ell}$ events will result in a high p_T $\ell\ell\not{E}_T$ final state. We note that the improvement by adding the $\ell^\pm\ell^\pm jj\not{E}_T$ selection is minimal in this case. The 5σ discovery curves are compared with the theoretical cross sections in Fig. 17. With integrated luminosities of 2, and 30 fb^{-1}, the lighter chargino with mass up to 310 and 360 GeV can be discovered respectively.

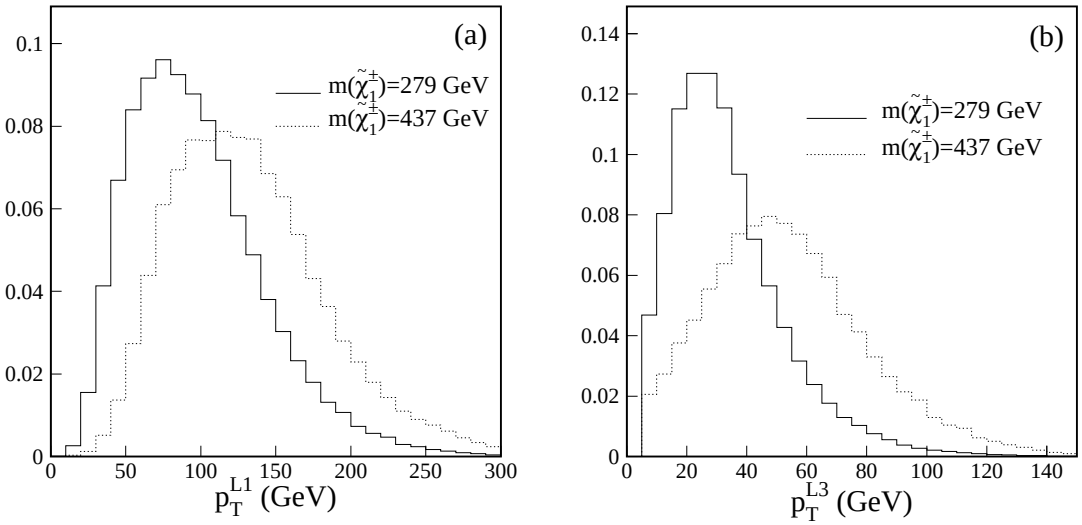

FIG. 16. The p_T distributions of (a) the leading lepton and (b) the third lepton for the models with a short-lived $\tilde{\ell}$ as the Co-NLSP for $m_{\tilde{\chi}_1^\pm} = 279,\ 437$ GeV ($\Lambda = 40,\ 60$ TeV). Note that the p_T requirement is 15 GeV for the leading lepton and 5 GeV for the non-leading leptons. All distributions are normalized to unit area.

Λ (TeV)	30	40	50	60	70
σ_{th} (fb)	121	24.5	6.7	2.3	0.9
$m_{\tilde{\chi}_1^\pm}$ (GeV)	197	279	358	437	517
$m_{\tilde{\ell}}$ (GeV)	99	128	158	188	218
ϵ (%)	14.7	15.4	9.6	4.7	1.4
$N_s/\delta N_b$ (2 fb^{-1})	44	9.4	1.6	0.3	–
$N_s/\delta N_b$ (30 fb^{-1})	152	32	5.5	0.9	0.1

TABLE V. The theoretical cross section, $\tilde{\chi}_1^\pm$ and $\tilde{\ell}$ masses, detection efficiency of the $\ell\ell\ell j\not{E}_T$ selection criteria, and significances for different values of Λ for the models with short-lived $\tilde{\ell}$'s as the Co-NLSP. The efficiencies typically have a relative statistical uncertainty of 4%. The observable background cross section is assumed to be 0.3 fb with a 20% systematic uncertainty.

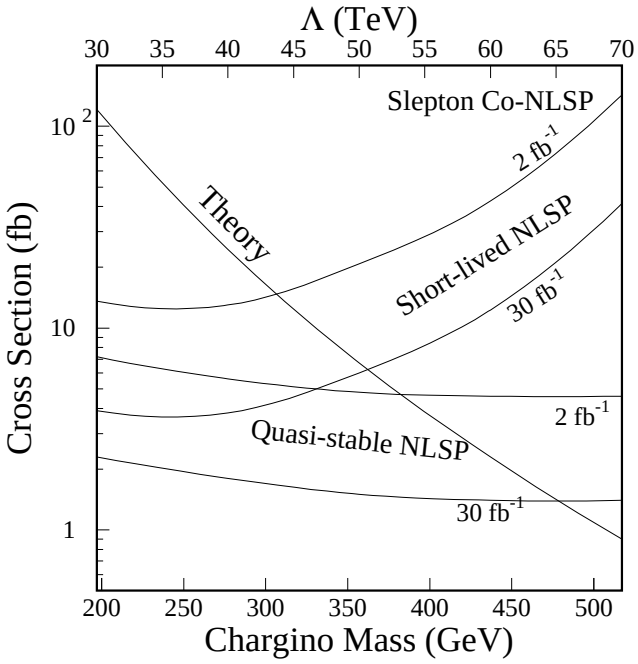

FIG. 17. The 5σ discovery cross section curves as functions of mass of the lighter chargino and the supersymmetry breaking scale Λ for the model line 3 along with the theoretical cross sections. The 5σ curves are shown for both short-lived and quasi-stable $\tilde{\ell}$ Co-NLSP's and for integrated luminosities of 2, 30 fb^{-1}.

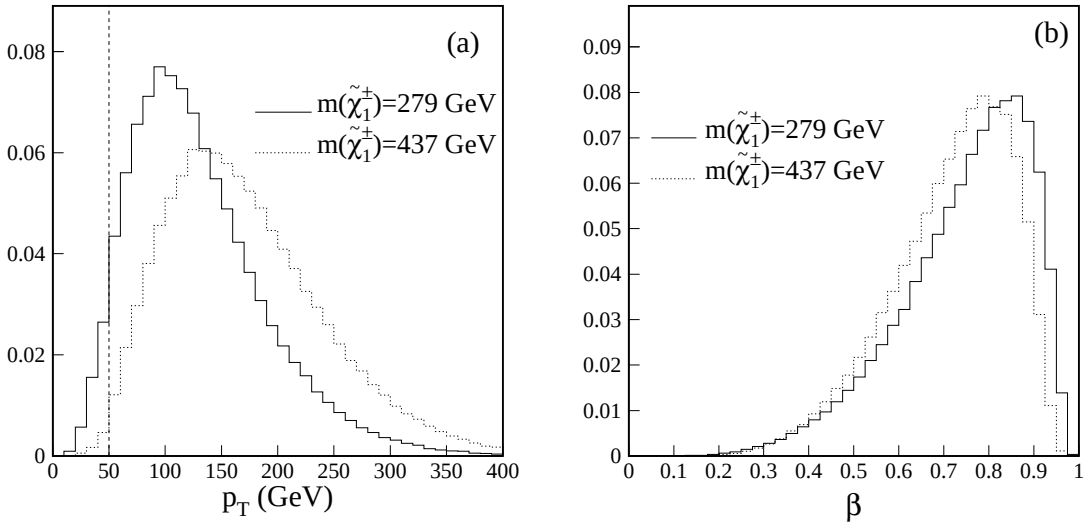

FIG. 18. The lepton p_T (a) and the NLSP speed β (b) distributions expected for models with a quasi-stable $\tilde{\ell}$ as the Co-NLSP for $m_{\tilde{\chi}_1^{\pm}} = 279,\ 437$ GeV ($\Lambda = 40, 60$ TeV), where β is measured in the unit of the speed of light c. The vertical dashed line indicates the cutoff. All distributions are normalized to unit area.

2. Quasi-stable $\tilde{\ell}$

If the $\tilde{\ell}$ has a long lifetime, it can decay outside the detector ($\gamma c\tau \gtrsim 3$ m). In this case, the $\tilde{\ell}$ will appear in the detector like a 'muon' except that the ionization energy loss will be large. This signature is identical to that of a quasi-stable $\tilde{\tau}_1$ discussed above. Therefore, the signal events can be identified using the $\ell\ell + dE/dx$ selection. The expected p_T and β distributions of the $\tilde{\ell}$ for $\Lambda = 40,\ 60$ TeV are shown in Fig. 18. The $\tilde{\ell}$s typically have very large p_T and are mostly central. For example, about 90% of the $\tilde{\ell}$s are in central pseudorapidity region with the tracking coverage for the case of $\Lambda = 70$ TeV. Table VI shows the detection efficiencies and the expected significances for different Λ values. The 5σ discovery curves are shown in Fig. 17. The lighter chargino mass discovery reach is about 390 GeV for $\mathcal{L}$=2 fb^{-1} and 480 GeV for $\mathcal{L}$=30 fb^{-1}.

D. Model Line 4: $\tilde{h}$ as the NLSP

For most of the parameter space, $\tilde{\chi}_1^0$ will predominantly decay to $\gamma\tilde{G}$ if it is the NLSP. However if $\tilde{\chi}_1^0$ is higgsino-like ($\tilde{h}$), $\tilde{\chi}_1^0 \to Z\tilde{G}$ and $\tilde{\chi}_1^0 \to h\tilde{G}$ decays could have significant branching ratios in some regions of the parameter space of non-minimal GMSB models. For the Run II studies, these models are defined to have fixed values of

$$N = 2, \quad \frac{M_m}{\Lambda} = 3, \quad \tan\beta = 3, \quad \frac{\mu}{M_1} = -0.75$$

with Λ varying. Here M_1 is the mass parameter associated with the $U(1)_Y$ symmetry. In these models, the lightest neutral higgs boson h has a mass around 104 GeV. Pair production

Λ (TeV)	30	40	50	60	70
σ_{th} (fb)	121	24.5	6.7	2.3	0.9
$m_{\tilde{\chi}_1^\pm}$ (GeV)	197	279	358	437	517
$m_{\tilde{\ell}}$ (GeV)	99	128	158	188	218
ϵ (%)	34.8	45.2	52.6	54.9	55.1
$N_s/\delta N_b$ (2 fb^{-1})	83	22	7.0	2.6	1.0
$N_s/\delta N_b$ (30 fb^{-1})	257	68	21	7.8	3.1

TABLE VI. The theoretical cross section, $\tilde{\chi}_1^\pm$ and $\tilde{\ell}$ masses, detection efficiency of the $\ell\ell$+dE/dx selection, and significances for different values of Λ for the models with quasi-stable $\tilde{\ell}$'s as the Co-NLSP. The relative statistical error on the efficiency is typically 1%. The background cross section is assumed to be 0.5 fb with a systematic uncertainty of 20%.

of supersymmetric particles may result in $\tilde{\chi}_1^0\tilde{\chi}_1^0 \to \gamma\tilde{G}\ h\tilde{G} \to \gamma b\bar{b}\tilde{G}\tilde{G}$ final state which would appear as $\gamma b\bar{b}\not{E}_T$ events in the detector assuming prompt $\tilde{\chi}_1^0$ decays. These events are characterized by high E_T photons and large $\not{E}_T$ as shown in the Fig. 19 for $\Lambda = 80, 110$ TeV. They can be selected using the $\gamma bj\not{E}_T$ selection criteria discussed in Section III B. The detection efficiencies and $N_s/\delta N_b$ significances are shown in Table VII for different values of Λ. Most of the events selected are due to the γh production with $h \to b\bar{b}$. However, a non-negligible fraction of the events is actually due to the $\gamma Z + X$ with $Z \to b\bar{b}$. The discovery reach in Λ and $m_{\tilde{\chi}_1^\pm}$ is shown in Fig. 20 for $\mathcal{L}$=2, 30 fb^{-1}.

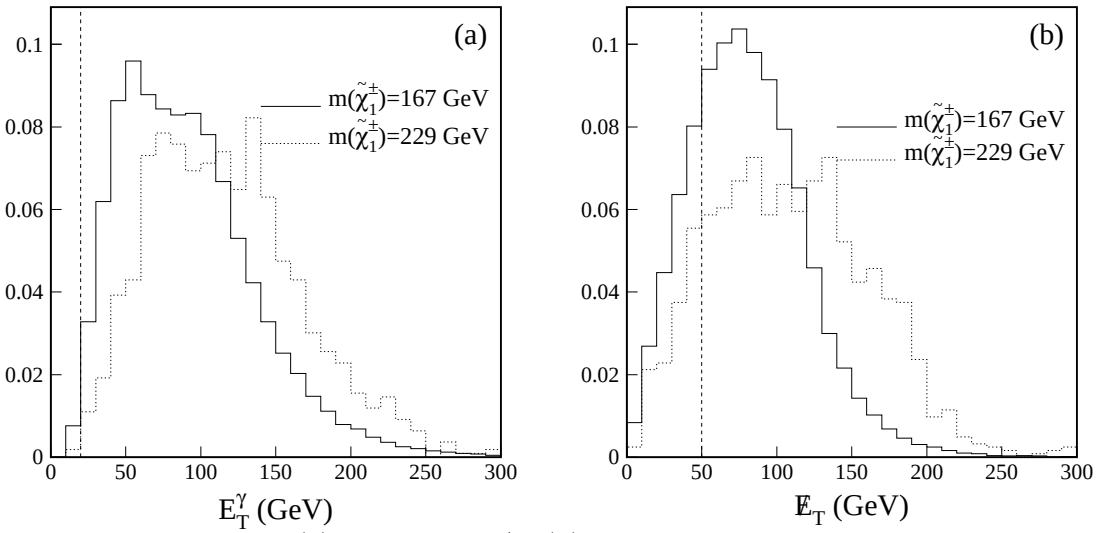

FIG. 19. The photon E_T (a) and event $\not{E}_T$ (b) distributions for models with a short-lived higgsino-liked $\tilde{\chi}_1^0$ as the NLSP with $m_{\tilde{\chi}_1^\pm} = 167,\ 229$ GeV ($\Lambda = 80,\ 110$ TeV). All distributions are normalized to have unit area.

If an excess is seen in the $\gamma bj\not{E}_T$ final state, it will be of great interest to reconstruct the di-jet invariant mass. Figure 21 shows the invariant mass distribution of the two leading jets for $\Lambda = 80$ TeV and $\mathcal{L}$=2 fb^{-1}. A mass peak around $m_h = 104$ GeV is clearly identifiable. The asymmetry in the mass distribution is partly due to $\gamma Z + X$ contribution and partly

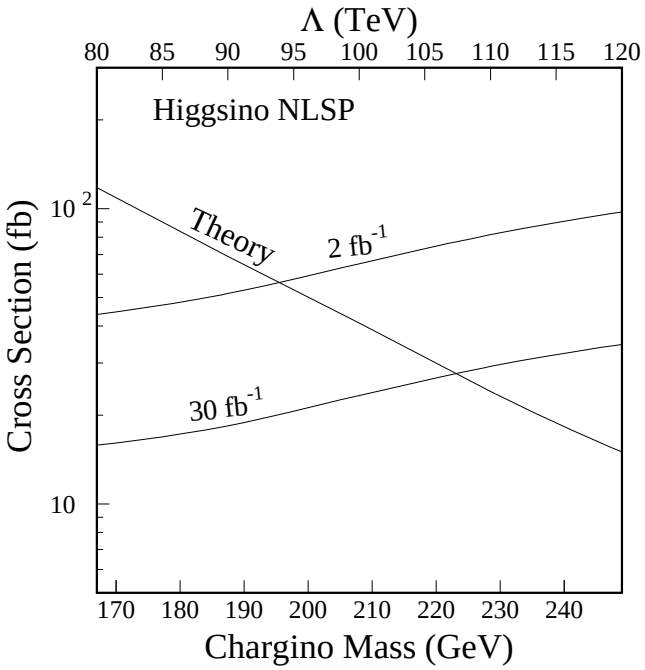

FIG. 20. The 5σ discovery cross section curves as functions of the supersymmetry breaking scale Λ and the lighter chargino mass for the model line 4 along with the theoretical cross sections. The $\tilde{h}$ is assumed to be short-lived.

Λ (TeV)	80	90	100	110	120
σ_{th} (fb)	118	69	41	24	15
$m_{\tilde{\chi}_1^\pm}$ (GeV)	167	188	208	229	249
$m_{\tilde{\chi}_1^0}$ (GeV)	154	176	197	218	239
m_h (GeV)	103	104	105	105	106
$\mathrm{Br}(\tilde{\chi}_1^0 \to \gamma\tilde{G})$	0.38	0.21	0.15	0.10	0.08
$\mathrm{Br}(\tilde{\chi}_1^0 \to h\tilde{G})$	0.38	0.52	0.59	0.63	0.66
ϵ (%)	8.0	6.8	5.4	4.3	3.6
$N_s/\delta N_b$ (2 fb^{-1})	13	6.7	3.2	1.5	0.8
$N_s/\delta N_b$ (30 fb^{-1})	38	19	8.9	4.1	2.2

TABLE VII. The theoretical cross section, $\tilde{\chi}_1^\pm$ and h masses, $\tilde{\chi}_1^0$ decay branching ratios, detection efficiency of the $\gamma bj\not{E}_T$ selection, and significances for different values of Λ for the models with a short-lived higgsino as the NLSP. The relative statistical error on the efficiency is typically 4%. The background cross section is assumed to be 0.9 fb with a 20% systematic error.

due to the effect of gluon radiation and the energy outside the jet cone.

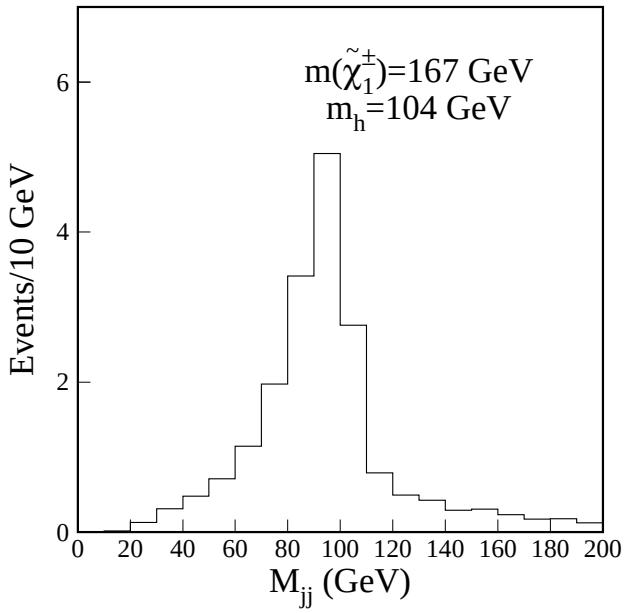

FIG. 21. The invariant mass distribution of the two leading jets for $m_{\tilde{\chi}_1^{\pm}} = 167$ GeV ($\Lambda = 80$ TeV) and $\mathcal{L}$=2 fb^{-1}. Note that 19 signal and less than 2 background events are expected.

V. SUMMARY

In this paper, observable background cross sections for the six final states in which new physics might manifest itself are estimated. All the final states studied are found to have small backgrounds. Implications of the analyses of these final states for future Tevatron runs are discussed in the framework of Gauge Mediated Supersymmetry Breaking models. Potential discovery reaches in supersymmetry parameter space for integrated luminosities of 2 and 30 fb^{-1} are examined for models with different NLSP. Though the selection criteria are not optimized for the models discussed and not all final states are investigated, the study does show that the upgraded DØ experiment at the improved Tevatron collider has great potentials for discovery.

VI. ACKNOWLEDGEMENT

The author would like to thank D. Cutts, K. Del Signore, G. Landsberg, S. Martin, H. Montgomery, S. Thomas, D. Toback, A. Turcot, H. Weerts, and J. Womersley for their assistance in the course of this study and/or their critical reading of this writeup and X. Tata for pointing out a mistake in one of the background estimations.

[1] See the workshop web page: `http://fnth37.fnal.gov/susy.html`.
[2] See for example S. Dimopoulos, S. Thomas, and J.D. Wells, Nucl. Phys. B **488**, 39 (1997); G.F. Guidice and R. Rattazzi, `hep-ph/9801271`; and the references therein.
[3] DØ Collaboration, S. Abachi *et al.*, Fermilab Pub-96/357-E.
[4] F. Paige and S. Protopopescu, BNL Report No. 38304, 1986 (unpublished), releases v7.37 and v7.42.
[5] D. Cutts and G. Landsberg, private communication.
[6] Yu. Gershtein, "*Level-1 Trigger for Slow Moving Particles*", DØnote # 3431.
[7] DØ Collaboration, B. Abbott *et al.*, Phys. Rev. Letters, **80**, 442 (1998).
[8] DØ Collaboration, B. Abbott *et al.*, Phys. Rev. Letters, **82**, 42 (1999).
[9] T. Han and R. Sobey, Phys. Rev. D **52**, 6302 (1995).
[10] DØ Collaboration, B. Abbott *et al.*, Phys. Rev. Letters, **80**, 1591 (1998).